Organic Electronics 75 (2019) 105319

Contents lists available at ScienceDirect

Organic Electronics

journal homepage: www.elsevier.com/locate/orgel

Low-threshold triple-wavelength lasing from a subwavelength triangle microcavity polymer laser fabricated by imaging holography

Wenbin Huang[a], Jing Wang[a], Yanjun Liu[c], Yan Ye[a], Linsen Chen[a], Zhi-gang Zheng[a,b,*], Yan-Hua Liu[a,**]

[a] School of Optoelectronic Science and Engineering & Collaborative Innovation Center of Suzhou Nano Science and Technology, Soochow University, Suzhou, 215006, China
[b] Department of Physics, East China University of Science and Technology, Shanghai, 200237, China
[c] Department of Electrical and Electronic Engineering, Southern University of Science and Technology, Shenzhen, 518055, China

ARTICLE INFO

Keywords:
Microcavities
Multi-wavelength microlaser
Imaging holography
Forster energy transfer
Distributed feedback resonance

ABSTRACT

We propose and demonstrate a low-threshold triple-wavelength polymer laser based on an elaborately designed subwavelength triangle microcavity with high optical confinement. The triangle optical microcavity in three different periodicities is fabricated in a one-step and versatile way by imaging holography. A collimated laser light (for illumination) sheds on a micrometer-scale diffractive optical element (as the object), and diffracted beams are collected by an objective lens (for imaging) and they interfere at the imaging plane, yielding the subwavelength triangle microcavity (as the image) with a demagnification ratio of 100. A novel conjugated polymer blend featuring efficient Förster energy transfer was investigated in detail for its potential as the gain medium. The blended conjugated polymer was overcoated onto the microcavity and lasing at wavelengths of 624.2 nm, 626.3 nm and 630.7 nm was simultaneously observed at a low pump threshold of 1.5 kW/cm^2. The imaging holography technique provides a flexible approach to yield optical microcavities in constructing multi-wavelength lasers.

1. Introduction

Multi-wavelength lasers have been extensively investigated for their potential applications in wavelength-division-multiplexing communication systems [1,2], high-precision refractometry sensing [3,4], optical clocks [5] and molecular fingerprinting [6]. The erbium doped fiber (EDF) as the gain medium has been exploited in multi-wavelength lasers for its wide gain spectrum and high gain coefficients. Multi-wavelength EDF ring lasers are demonstrated using a triple-transmission-band fiber Bragg grating filter [7], dual-pass Mach–Zehnder interferometer [8] or a double-ring structure with hybrid gain medium [9], and a configuration of multiple EDF amplifiers [10]. However, since EDF is a homogenous gain medium, the fiber lasers based on EDF often suffer from strong mode competition and unstable multi-wavelength lasing at room temperature. On the other hand, semiconductor optical amplifiers, possessing properties of primarily inhomogeneous broadening and broad gain spectrum, have been exploited for producing in multi-wavelength lasers in the fiber configuration [11] or in laser arrays by constructing vertical cavity surface-emitting lasers using high-contrast gratings as top mirrors [12], distributed feedback lasers using the reconstruction-equivalent chirp technique [13] and surface emitting quantum lasers using distributed Bragg reflectors [14].

When compared with the inorganic gain media, the organic counterparts, such as the dye or the organic semiconductor, have advantages of mechanical flexibility, ease for chemical modification and solution processability [15–17]. In addition, they also exhibit broad gain spectra, large absorption cross-sections and high fluorescence efficiencies, showing prospect for realizing high performance multi-wavelength lasers. As a result, multi-wavelength organic lasers are reported in different resonator configurations. For example, multi-wavelength laser emission from the dye-doped cholesteric liquid crystal was demonstrated by adding oversaturated chiral dopant into the mixture [18] or by an inhomogeneous curing of the dye-doped cholesteric polymer film [19], of both are attributed to a variation of the helical pitch of the cholesteric liquid crystal domains. Dual-wavelength lasing was observed in dye-doped holographic polymer dispersed liquid

* Corresponding author. Department of Physics, East China University of Science and Technology, Shanghai, 200237, China.
** Corresponding author. School of Optoelectronic Science and Engineering & Collaborative Innovation Center of Suzhou Nano Science and Technology, Soochow University, Suzhou, 215006, China.
E-mail addresses: zgzheng@ecust.edu.cn (Z.-g. Zheng), yhliu@suda.edu.cn (Y.-H. Liu).

https://doi.org/10.1016/j.orgel.2019.06.031
Received 18 May 2019; Received in revised form 17 June 2019; Accepted 23 June 2019
Available online 26 July 2019

crystal gratings by a careful match of the gain spectrum and the Bragg feedback at different orders [20], and one may not vary the lasing wavelength separately. A triple-wavelength polymer laser was further demonstrated by a direct recording of the triangular-lattice photonic crystal into the active film, and tunability is demonstrated by mechanically bending the substrate [21].

Apart from the gain media, the fabrication of cavities with multiple-mode emission capability is another issue in determining performance of the multi-wavelength laser. Microcavities, such as the ring with the whispering gallery mode effect [22], the one-dimensional grating with the distributed feedback effect [23], the photonic crystal with the bandgap effect [24], etc., providing strong light confinement by the resonant recirculation are frequently used in realizing multi-wavelength lasers. The multi-wavelength EDF ring lasers utilized the ring cavity formed during fiber formation, have the advantage of high laser power, however, extra mode selection mechanisms such as the Bragg filter or the Mach–Zehnder interferometer have to be added for stable laser operation, leading to a complicated fabrication process. The inorganic semiconductor laser arrays consist of multiple microlasers working in different wavelengths and could emit multiple lasing in a controllable manner. Each microlaser cavity, composed of a photonic crystal or a high-refractive index grating, has to be made with high wavelength spacing precision, and particle beam lithography or multiphoton lithography techniques with the finest resolution have to be utilized, exhibiting difficulties for large-area production [13,25,26]. The photonic crystal with different periodicities in different directions could also support multiple mode resonation and emits multi-wavelength lasing [27,28], however, it requires multiple holographic exposure with a delicate control of parameters in each step, leading to complexity in fabrication and uncertainty in device performance. In addition, the self-assembled helical superstructure from liquid crystal molecules as the laser cavity is at low-cost and cavity parameters are tunable with multiple external stimuli, such as the electric field, the optical field, etc. [29], however, there are often detects during the formation of the superstructures, leading to deterioration of device performance.

In this work, we propose and demonstrate a triple-wavelength polymer microlaser by using a subwavelength triangle microcavity as the resonator. A novel mixture containing a blue-emitting conjugated polymer as the host material and a red-emitting one as the guest is chosen as the gain media. The blue-emitting conjugated polymer works as the efficient absorption material for light utilization. The energy levels of the two materials are specifically optimized to obtain a large spectral overlap between the fluorescence spectrum of the host and the absorption spectrum of the guest, resulting in efficient energy transfer via nonradioactive processes. The guest material is apt to return to the ground energy level via simulated emission, furnishing high optical gain. In this way, the self-absorption is reduced and the gain spectrum is expanded, which is beneficial to fabricate low-threshold multi-wavelength lasers. Moreover, we have employed a low-cost and versatile fabrication technique called imaging holography for one-step fabrication of subwavelength microcavities with triple-mode characteristics. This elaborately designed optical microcavity has never been reported and exhibits strong photon confinement effects for efficient multi-wavelength generation. In the novel imaging holography technique, a master diffractive optical element (DOE, as the object) is illuminated by a collimated laser beam to produce multiple diffracted beams. The diffracted beams are then collected and focused by an objective lens (for imaging). At the focal plane, these beams will then overlap and interfere with each other to yield a subwavelength microcavity with demagnification to the DOE (as the image). The multi-mode characteristics, such as the lasing wavelength, the wavelength spacing and the number of lasing modes, of the microlaser could be easily varied by engineering the subwavelength microcavity parameters, offering versatile and controllable coherent light sources for photonic integration chip applications.

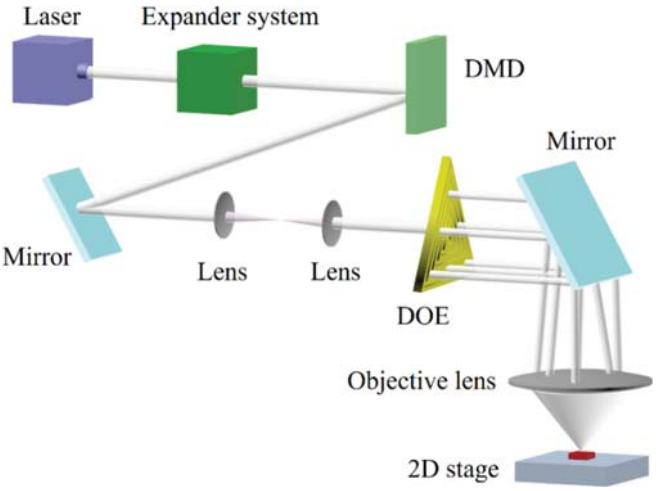

Fig. 1. Experimental setup of the imaging holography technique. The DOE splits the recording laser into multiple beams which are collected by the objective lens. These beams interfere at the imaging plane, yielding the pattern for photo-recording. The light field pattern is an image to the DOE with a demagnification rate determined by the objective lens. This setup could generate various kinds of structured light illumination for photolithography simply by varying the DOE. The 2D stage distributes the patterns over the sample on demand.

2. Materials and methods

2.1. The triangle optical microcavity by imaging holography

The developed imaging holography technique could generate various kinds of structured light illumination for the photo-recording of subwavelength microcavities and is based on the double Fourier transformation principle. The experimental setup is depicted in Fig. 1, where a pulsed UV laser beam (Advanced Optowave Corporation. Wavelength: 355 nm; repetition rate: 1 kHz) is collimated by an expander system, shaped by a digital micromirror device, and then passes through a 4f imaging system and impinges onto the DOE. The DOE pattern has micrometer-scale features and it will diffract the single laser beam into multiple ones and only ± 1st orders are allowed to pass through the objective lens. They will then overlap and interfere with each other at the focal plane to produce the structured light illumination. We have carried out theoretical calculations (see Method Details) and found that the structured light pattern is directly imaged from the DOE pattern, with a demagnification ratio of $2M$ where M is the magnification ratio of the objective lens. The imaging holography equation is not infinitely correct and we have further derived the resolution of the imaging holography technique to be $\lambda/4NA$, where λ is the lasing wavelength and NA is the numerical aperture of the objective lens. In this work, we have utilized an objective lens with a NA of 0.85, leading to a theoretical low-limit of the linewidth around 110 nm. Single laser pulse generates the whole structured light illumination for the photo-recording of a complete subwavelength microcavity, featuring ultra-high fabrication efficiency. In addition, the 2D stage is controlled to precisely (error around 100 nm) distribute the structured light fields on the recording medium, and thus this fabrication technique is quite advantageous in terms of parallel microcavity integration for on-chip applications. Various kinds of structured light illumination with nanometer features could be generated by redesigning the DOEs and could be distributed precisely onto the sample on demand. However, to obtain diffractive beams by the DOE component, it requires periodic structures in different directions (one periodicity in one direction), giving rise to a limitation on the achievable types of microcavities.

In order to fabricate an optical microcavity supporting triple-mode

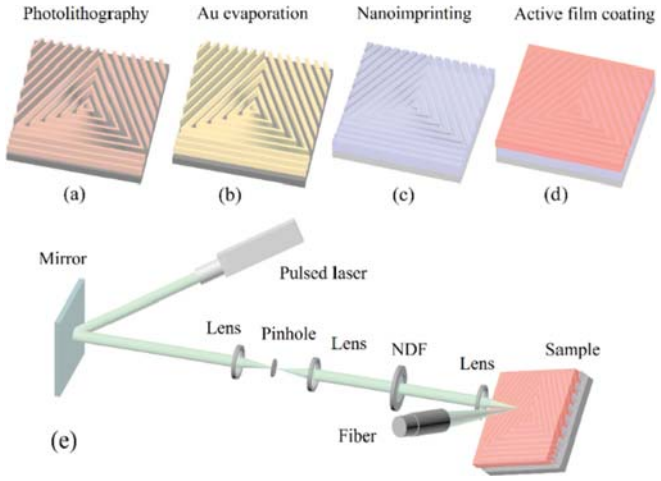

Fig. 2. Triple-wavelength polymer laser fabrication and characterization. (a) Photo-patterning the photo-resist using the structured light field. The relief nanostructure forms after development. (b) Mold fabrication by a direct evaporation of an Au layer onto the photo-resist relief nanopattern to lower the surface free energy for nanoimprinting. (c) Replication of the pattern into the adhesive by using the photo-resist pattern as the mold. (d) Microlaser fabrication by overcoating the active polymer onto the relief pattern. (e) Experimental setup for pumping the microlaser.

resonation, we have specifically designed a DOE with three periodicities in three directions and its configuration is shown schematically in Fig. 1. It consists of periodic lines in three directions and is quite different from the triangle-lattice photonic crystal composed of periodic dots aligned in three directions. This particular cavity is expected to concentrate the light field in the microcavity center and provides ultra-high light confinement. For fabrication, the laser direct writing technique is used to write the pattern into the positive photoresist with the line periodicity in three directions being 40.0 μm, 40.2 μm and 40.4 μm, respectively. The DOE pattern was then etched into the silica substrate with a depth of 380 nm to eliminate the 0th-order transmission at the operating wavelength, where the photoresist serves as the mask. Finally, the patterned silica DOE was cleaned and placed in the optical setup. In order to obtain a subwavelength optical microcavity, we have employed an objective lens with a high magnification ratio of 50. The six beams diffracted from the DOE was collected and they interfere at the imaging plane. The structured light field was used to photo-pattern the positive photoresist (Thickness ~200 nm, Suzhou Ruihong Electronic Chemical Co., Ltd.) on the silica substrate and yield the relief nanopattern after development (Fig. 2(a)).

2.2. Microlaser fabrication and characterization

For microlaser fabrication, we first evaporated a thin Au layer onto the photoresist relief nanopattern to lower the surface free energy (Fig. 2(b)). The relief nanopattern was then brought into contact with UV curable adhesive on a flexible substrate and was subsequently cured via a UV light-emitting diode, after that the mold was detached from the substrate, leading to the replicated pattern on the flexible substrate (Fig. 2(c)). The host and guest conjugated polymers were chosen as the blue-emitting PFO (Poly(9,9-dioctylfluorene), Sigma Aldrich, MW 20,000) and the red-emitting MDMO-PPV ([2-methoxy-5-(3′,7′-dimethyloctyloxy)]-1,4-phenylenevinylene), Sigma Aldrich, MW 100,000), respectively. The Förster energy transfer (FRET) material mixture was dissolved in toluene at a fixed concentration of 1.2 wt %, with the ratio between the host and the guest being varied (from 10:0.5 to 10:4) to investigate the FRET process. The blended conjugated polymer was overcoated onto the relief pattern to complete the microlaser (Fig. 2(d)). For optical excitation, a pulsed laser beam with the

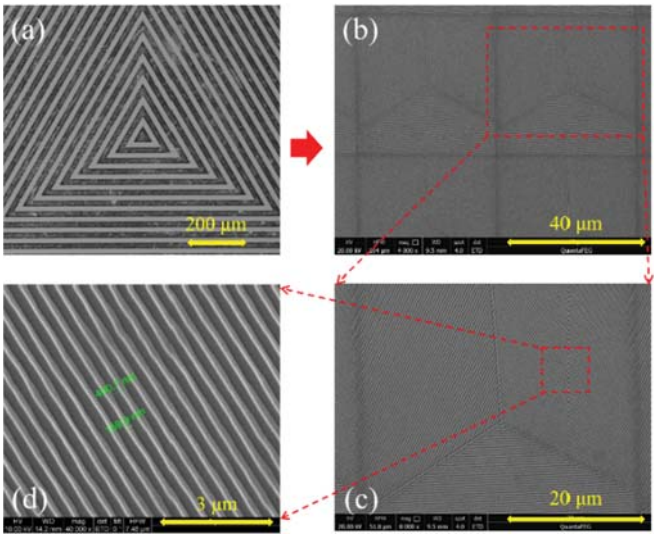

Fig. 3. (a) Optical microscope image of the DOE, (b) SEM image of several triangle optical microcavity, (c) SEM image of single triangle optical microcavity and (d) SEM image showing the subwavelength lines in one microcavity.

working wavelength of 349 nm and the pulse width of 8 ns was focused into a strip and a spot for amplified spontaneous emission (ASE) and lasing investigations, respectively. A set of neural density filters (NDF) was inserted in the optical path to control the pump intensity. In the case of the ASE characterization, an adjustable slit was used to control the strip length in order to calculate the film gain coefficient through the variable strip length (VSL) method, where the conjugated polymer film was utilized without adding the microcavity. Edge Emission was collected as light was amplified along the pumping length. In the case of spot pumping, normal emission to the sample surface was collected and analyzed by a fiber coupled spectrometer with the resolution of 0.19 nm (Avaspec) (Fig. 2(e)). Although the light feedback direction is in the sample plane, emission can be outcoupled via the subwavelength tri-directional periodic lines.

3. Results and discussions

3.1. The subwavelength triangle optical microcavity

Fig. 3(a) shows the microscope image of the DOE used in this work for the fabrication of the subwavelength microcavity via imaging holography. It consists of tri-directional periodic lines for triple-mode resonance. Fig. 3(b) shows the scanning electron microscope (SEM) image of the patterned microcavities on the photoresist after development. The whole sample was densely distributed with triangle microcavities with a size of 40 μm. Our self-developed lithography system can complete patterning the sample into an area of 1 cm^2 in 5 min, demonstrating ultra-high fabrication efficiency. As expected, single triangle microcavity consists of tri-directional periodic subwavelength lines in accordance with the DOE pattern. Fig. 3(c) and (d) show more morphological details of the subwavelength microcavity. Theoretically, the periodicity of the microcavity in the three directions should be 400 nm, 402 nm and 404 nm, respectively. The three periodicities could support mode resonance at three different wavelengths, enabling a triple-wavelength microcavity. However, the periodicity measurement by SEM has insufficient resolution in determining each periodicity in accuracy and we have only measured the periodicity in one direction for reference which is shown in Fig. 3(d). The measured linewidth is 159.9 nm and the periodicity is 400.7 nm. Overall, the SEM observations and measurements agree well with theoretical predictions and confirm the excellent capability of the imaging holography technique in fabricating the triangle optical microcavities. It is worth noting that the

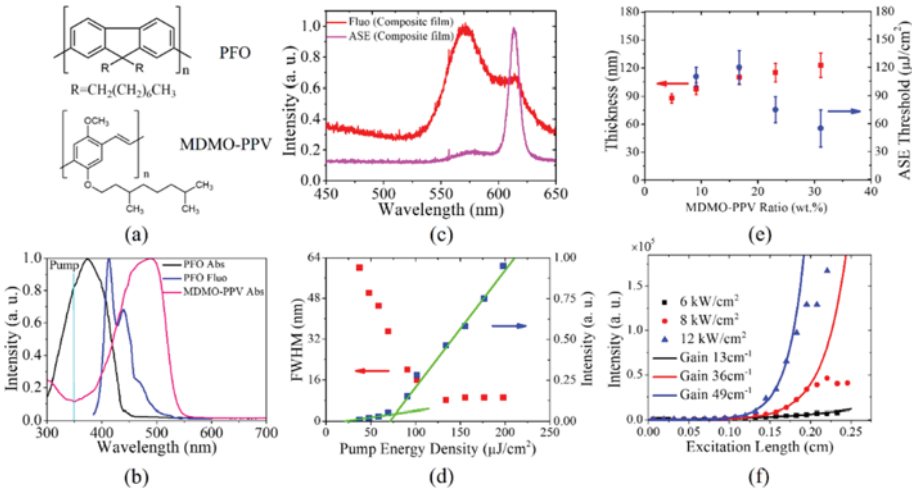

Fig. 4. (a) Molecular structures of the host and guest conjugated polymers. (b) The absorption and fluorescence spectra of the host (PFO) conjugated polymer and the fluorescence spectrum of the guest (MDMO-PPV) conjugated polymer. (c) Fluorescence and amplified spontaneous emission spectra of the blended conjugated polymer film. (d) The dependence of the FWHM and emission intensity as a function of the pumping intensity for the blended conjugated polymer films. (e) Composite film properties as a function of the guest material ratio. (f) Output edge emission intensity as a function of the excitation length for the blended conjugated polymer film under different pumping intensities. Solid lines are fitting curves based on the VSL method and the deduced gain coefficients are also shown. Fluo and ASE is the abbreviation of fluorescence and amplified spontaneous emission, respectively.

aspect ratio of the subwavelength pattern deviates slightly from that of the master DOE pattern, which could be mainly attributed to development conditions. In addition, high magnification SEM image of Fig. 3(d) shows that the linewidth of those periodic lines is not uniform with slight distortions. This should be attributed to the stitching error in fabricating the micrometer-scale DOE, which blurs the interference pattern of the multiple diffractive beams and hence deteriorates the quality of the formed subwavelength pattern.

3.2. The host-guest conjugated polymer as an efficient gain medium

As for the gain media, we take advantage of efficient FRET in a host-guest light emitting system to improve the lasing performance. The overlap between the fluorescence spectrum of the host material and the absorption spectrum of the guest material is crucial to ensure efficient energy transfer, although the process is non-irradiative. Fig. 4(a) shows the molecular structures of the host and guest conjugated polymers. Fig. 4(b) further shows the absorption and fluorescence spectra of the selected host (PFO) and guest (MDMO-PPV) materials. The red-emitting MDMO-PPV have not only high photoluminescence quantum efficiencies but also absorption bands that overlap completely with the emission spectrum of PFO, ensuring an efficient energy transfer from the host material to the guest one. In order to investigate the gain possibilities of the composite film, the fluorescence and ASE emission spectra from the composite film are shown in Fig. 4(c). The fluorescence spectrum consists of two peaks, which are attributed to the 0-0 and 0–1 vibrational peak of the guest emitter. At a higher pumping intensity, fluorescence emission evolves to ASE as a result of the optical amplifying effect at certain wavelengths, peaking at the 0–1 vibrational peak with the highest gain coefficient. It is also worth mentioning that there is almost no residual emission from the host conjugated polymer, demonstrating a complete energy transfer from the host to the guest. The full width at half maxima (FWHM) and the edge emission intensity as a function of the pumping intensity from the composite film is further given in Fig. 4(d). For FWHM, the broad emission band narrows significantly with the increase of pumping intensity, *i.e.*, gain narrowing, at low pumping intensity below a threshold. At the pumping intensity above the threshold, the FWHM of the emission spectra is about 10 nm, which keeps almost constant with the increase of the pumping intensity. This indicates that the spontaneous emission is gradually dominated by the stimulated emission as the pump intensity increases, as long-lived excitations are stimulated by photons propagating along the pumping length, demonstrating the gain capability of the composite film. The effect of the blend composition ratio on gain performance is shown in Fig. 4(e). The film thickness increases from 90 nm to 120 nm as the guest material ratio increases, due to the increased solution viscosity. The ASE threshold decreases with the increase in the guest material ratio and no optical gain can be experimentally observed when the guest concentration is below 5 wt%. The ASE threshold is essentially determined by two major factors in the FRET blend: the FRET efficiency and the self-quenching of the guest material, which are highly dependent on the concentration of the guest material [30]. It seems that the increase in the FRET efficiency due to the intensifying molecular interaction and the increased optical confinement as a result of the film thickness play a more important part role in determining the composite material performance.

We have further quantized the gain coefficients of the composite film with the host and guest material ratio being 10:4 by the VSL method. Under the strip pumping conditions, the edge emission intensity was measured as a function of the pumping length. The net gain coefficient was then calculated by fitting the experimental data to the expected dependence for ASE [31]:

$$I_{out} = \frac{AP_0}{g}[\exp(gl) - 1] \quad (1)$$

Where I_{out} is the edge emission intensity, A is a constant that stands for the spontaneous emission rate, P_0 is the pumping intensity, g is the gain coefficient and l is the pumping length. The parameters of A and g could be obtained by fitting the experimental data to the equation. For one set of the measurements, the pumping intensity remains unchanged, as the optical gain is directly related to the excitation intensity. Fig. 4(f) shows experimentally measured edge emission intensity as a function of the pump strip length, from which we can deduce the optical gain coefficients of the sample at different pumping intensities via the data fitting. The fitting curves using Eq. (1) are also shown, which yield the gain coefficients at corresponding pump intensities. The measured gain coefficient increases from 13 cm^{-1} to 49 cm^{-1} when the pump intensity changes from 6 kW/cm^2 to 12 kW/cm^2. The agreement between the fitting curves and experimental data deteriorates when the pump intensity increases, especially for the long pumping strip cases. This is mainly attributed to the optical saturation when propagating photons deplete a substantial fraction of excitation and the output emission intensity deviates from the theoretical equation. The achieved gain coefficients from the composite film are large enough to ensure excellent multi-wavelength laser performance [32].

3.3. Multi-wavelength lasing from the triangle optical microcavity

The triangle microcavity with tri-directional subwavelength lines is different from the grating or the photonic crystal configuration, however, we found that the periodic lines in one direction could be regarded as a distributed feedback laser, and thus the well-known Bragg

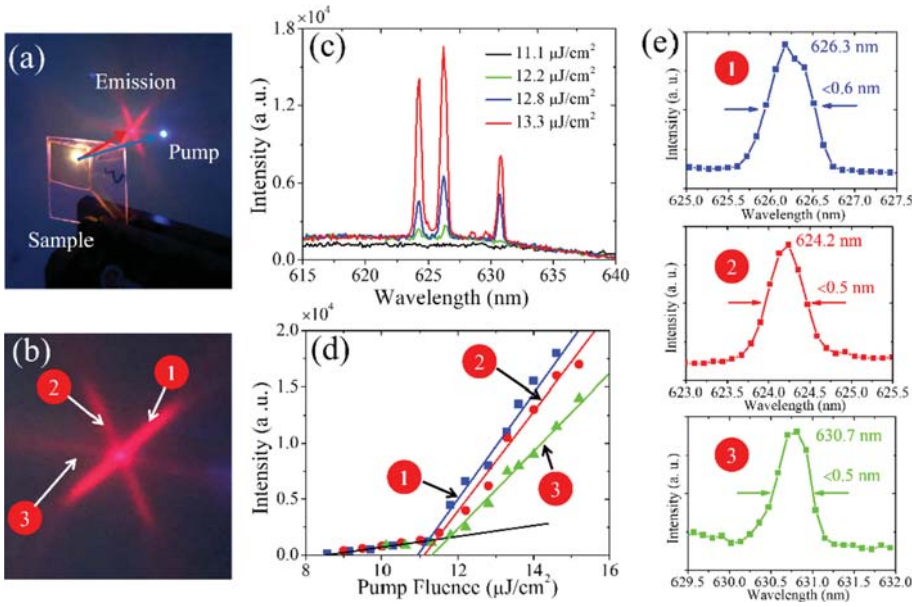

Fig. 5. Multi-wavelength microlaser performance. (a) Photograph of the microlaser under pumping. (b) An enlarged view of the laser spot. (c) Emission spectra from the triangle optical microcavity polymer microlaser under different pumping intensities. (d) Peak lasing intensity at three separate wavelengths as a function of the pumping intensity. (e) A zoomed view into the spectral profile of each lasing peak.

equation could be directly utilized to explain the feedback mechanism in this peculiar microcavity. As mentioned in the experimental part that the periodicities in three directions of the DOE is 40.0 μm, 40.2 μm and 40.4 μm, respectively. According the criterion of the imaging holography developed in this work, the structured light field at the imaging plane is an image to the DOE pattern with a demagnification ratio of 100, and thus the periodicities in different directions of the triangle microcavity is 400 nm, 402 nm and 404 nm accordingly. The Bragg equation:

$$2n_{eff}\Lambda = m\lambda \tag{2}$$

Where λ is the lasing wavelength, n_{eff} is the mode effective refractive index, Λ is the periodicity and m is the Bragg order. The Bragg order is 2 and the mode effective refractive index is around 1.55 according to the waveguiding theory, therefore, the three lasing wavelengths should locate around 625 nm with an average wavelength spacing of 3.2 nm. The lasing wavelength just falls in the ASE regime of the composite conjugated polymer film, ensuring a high optical gain.

Fig. 5(a) and (b) show the photograph of the lasing device and the emission pattern, respectively. When the pump energy was above the laser threshold, the sample emits the laser spot consisted of three bright lines, attributing to the out-coupling effect of the periodic subwavelength lines [33]. Each emission line corresponds to a feedback direction of the triangle microcavity, thereby rending a triple-wavelength operation. The emission spectra from the triangle microcavity laser at different pumping intensities are shown in Fig. 5(c). Under the low pump intensity (11.1 μJ/cm^2), the emission shows the broadband spontaneous emission. As the pump intensity increases, three lasing peaks appear and their intensity increases steadily, as shown in Fig. 5(d). There appears to be two regimes for the emission intensity. One is below the laser threshold, where the emission intensity is low and increases slowly with the pump intensity. The other is beyond the laser threshold, where the emission intensity undergoes an abrupt increase with the pump intensity. The different emission intensity dependence is attributed to the difference in the emission directionality of spontaneous emission and laser emission. The two regimes are quasi-linear and the laser threshold is deduced by the intersection of the two fitting liner curves. The laser thresholds for the three wavelengths is determined to be 11.3 μJ/cm^2, 11.5 μJ/cm^2 and 11.8 μJ/cm^2, respectively, attributing to the mode competition process in this microcavity. With the pump pulse duration being 8 ns, the power density threshold is around 1.5 kW/cm^2, much lower than that in previous publications on multi-wavelength organic lasers [21,27], indicating the effectiveness of the novel cavity in resonating light. It is believed that the design of the triple-wavelength microcavity with tri-directional subwavelength lines and the one-step fabrication with the imaging holography technique is crucial in realizing this low-threshold triple-wavelength polymer microlaser. The spectral profile of each laser peak was further given in Fig. 5(e). The FWHM of each lasing peak is around 0.5 nm which corresponds to a high Q factor around 1300, confirming the effectiveness of the peculiar microcavity in confining light. As a result, the polymer microlaser emits triple wavelength lasing at wavelengths of 624.2 nm, 626.3 nm and 630.7 nm, which agrees well with the prediction by the Bragg equation. It is also worth to note that, the imaging holography technique is versatile to provide multi-wavelength polymer microlasers, with a flexibility in designing the number of lasing modes and the location of each lasing wavelength by an elaborate design of the DOE.

4. Conclusions

In summary, we have proposed and demonstrated an low-threshold triple-wavelength polymer microlaser based on a specifically designed triangle optical microcavity. The triangle optical microcavity consists of tri-directional periodic lines with different periodicities, which could support effective light resonating at three separate modes. Furthermore, we employed an imaging holography technique for one-step fabrication of the subwavelength triangle optical microcavity, in which the structured light field for photo-recording was generated from a DOE pattern, with a demagnification ratio of 100, furnishing an efficient and versatile approach to subwavelength optical microcavities. The PFO and MDMO-PPV conjugated polymer serves as the efficient absorbers and emitters, and the matched energy levels facilitate an effective energy transfer, showing a gain coefficient of 49 cm^{-1}. The triangle microcavity laser emits stable three lasing at locations of 624.2 nm, 626.3 nm and 630.7 nm with a low pump threshold of 1.5 kW/cm^2. More important, the imaging holography technique could precisely distribute the microcavities over the recording medium, creating new possibilities for light modulation using on-chip or arrayed microcavities.

Acknowledgments

We acknowledge the financial support from National Natural Science Foundation of China (NSFC) (Grant Nos. 61575135, 61822504, 61575063, 51873060 and 61575132), the Natural Science Foundation

of Jiangsu Province (Grant No. BK20181166), China Postdoctoral Science Foundation (Grant No. 2017T100403), the National Science Foundation of the Jiangsu Higher Education Institutions of China (No. 18KJB510040), Shanghai Rising-Star Program (Grant No. 17QA1401100), and State Key Laboratory of Applied Optics (No. M200-D-1716).

References

[1] T. Healy, F.C.G. Gunning, A.D. Ellis, J.D. Bull, Multi-wavelength source using low drive-voltage amplitude modulators for optical communications, Opt. Express 15 (2007) 2981–2986.
[2] P.J. Smith, D.W. Faulkner, G.R. Hill, Evolution scenarios for optical telecommunication networks using multiwavelength transmission, Proc. IEEE 81 (1993) 1580–1587.
[3] A.L. Chaudhari, A.D. Shaligram, Multi-wavelength optical fiber liquid refractometry based on intensity modulation, Sensor Actuat. A-Phys. 100 (2002) 160–164.
[4] J. Marshall, G. Stewart, G. Whitenett, Design of a tunable L-band multi-wavelength laser system for application to gas spectroscopy, Meas. Sci. Technol. 17 (2006) 1023.
[5] D. Pudo, M. Depa, L.R. Chen, Single and multiwavelength all-optical clock recovery in single-mode fiber using the temporal Talbot effect, J. Light. Technol. 25 (2007) 2898–2903.
[6] J.R. Lucio-Gutiérrez, J. Coello, S. Maspoch, Enhanced chromatographic fingerprinting of herb materials by multi-wavelength selection and chemometrics, Anal. Chim. Acta 710 (2012) 40–49.
[7] L. Xia, P. Shum, Y. Wang, T.H. Cheng, Stable triple-wavelength fiber ring laser with ultranarrow wavelength spacing using a triple-transmission-band fiber Bragg grating filter, IEEE Photonics Technol. Lett. 18 (2006) 2162–2164.
[8] A.-P. Luo, Z.-C. Luo, W.-C. Xu, Tunable and switchable multiwavelength erbium-doped fiber ring laser based on a modified dual-pass Mach-Zehnder interferometer, Opt. Lett. 34 (2009) 2135–2137.
[9] Z. Chen, S. Ma, N.K. Dutta, Multiwavelength fiber ring laser based on a semiconductor and fiber gain medium, Opt. Express 17 (2009) 1234–1239.
[10] Z.G. Lu, C.P. Grover, A widely tunable narrow-linewidth triple-wavelength erbium-doped fiber ring laser, IEEE Photonics Technol. Lett. 17 (2005) 22–24.
[11] Z. Zhang, J. Wu, K. Xu, X. Hong, J. Lin, Tunable multiwavelength SOA fiber laser with ultra-narrow wavelength spacing based on nonlinear polarization rotation, Opt. Express 17 (2009) 17200–17205.
[12] V. Karagodsky, B. Pesala, C. Chase, W. Hofmann, F. Koyama, C.J. Chang-Hasnain, Monolithically integrated multi-wavelength VCSEL arrays using high-contrast gratings, Opt. Express 18 (2010) 694–699.
[13] J. Lu, S. Liu, Q. Tang, H. Xu, Y. Chen, X. Chen, Multi-wavelength distributed feedback laser array with very high wavelength-spacing precision, Opt. Lett. 40 (2015) 5136–5139.
[14] P. Jouy, C. Bonzon, J. Wolf, E. Gini, M. Beck, J. Faist, Surface emitting multi-wavelength array of single frequency quantum cascade lasers, Appl. Phys. Lett. 106 (2015) 071104.
[15] V.G. Kozlov, V. Bulović, P.E. Burrows, S.R. Forrest, Laser action in organic semiconductor waveguide and double-heterostructure devices, Nature 389 (1997) 362.
[16] J. Clack, G. Lanzani, Organic photonics for communications, Nat. Photonics 4 (2010) 438.
[17] I.D.W. Samuel, G.A. Turnbull, Organic semiconductor lasers, Chem. Rev. 107 (2007) 1272–1295.
[18] C.-T. Wang, T.-H. Lin, Multi-wavelength laser emission in dye-doped photonic liquid crystals, Opt. Express 16 (2008) 18334–18339.
[19] Y. Huang, S.-T. Wu, Multi-wavelength laser from dye-doped cholesteric polymer films, Opt. Express 18 (2010) 27697–27702.
[20] Z. Diao, S. Deng, W. Huang, L. Xuan, L. Hu, Y. Liu, J. Ma, Organic dual-wavelength distributed feedback laser empowered by dye-doped holography, J. Mater. Chem. 22 (2012) 23331–23334.
[21] T. Zhai, Y. Wang, L. Chen, X. Zhang, Direct writing of tunable multi-wavelength polymer lasers on a flexible substrate, Nanoscale 7 (2015) 12312–12317.
[22] X.-F. Jiang, C.-L. Zou, L. Wang, Q. Gong, Y.-F. Xiao, Whispering-gallery microcavities with unidirectional laser emission, Laser Photonics Rev. 10 (2015) 40–61.
[23] W. Huang, Z. Diao, Y. Liu, Z. Peng, C. Yang, J. Ma, L. Xuan, Distributed feedback polymer laser with an external feedback structure fabricated by holographic polymerization technique, Org. Electron. 13 (2012) 2307–2311.
[24] A. Tandaechanurat, S. Ishida, D. Guimard, M. Nomura, S. Iwamoto, Y. Arakawa, Lasing oscillation in a three-dimensional photonic crystal nanocavity with a complete bandgap, Nat. Photonics 5 (2010) 91–94.
[25] C. Wang, L. Yang, Y. Hu, S. Rao, Y. Wang, D. Pan, S. Ji, C. Zhang, Y. Su, W. Zhu, J. Li, D. Wu, J. Chu, ACS Nano 13 (2019) 4667–4676.
[26] D. Wu, S.Z. Wu, J. Xu, L.G. Niu, K. Midorikawa, K. Sugioka, Laser Photonics Rev. 8 (2014) 458–467.
[27] W. Huang, D. Pu, W. Qiao, W. Wan, Y. Liu, Y. Ye, S. Wu, L. Chen, Tunable multi-wavelength polymer laser based on a triangular-lattice photonic crystal structure, J. Phys. D Appl. Phys. 49 (2016) 335103.
[28] H. Wu, Y. Jiao, C. Zhang, C. Chen, L. Yang, J. Li, J. Ni, Y. Zhang, C. Li, Y. Zhang, S. Jiang, S. Zhu, Y. Hu, D. Wu, J. Chu, Nanoscale 11 (2019) 4803–4810.
[29] Z.-g. Zheng, B.-w. Liu, L. Zhou, W. Wang, W. Hu, D. Shen, Wide tunable lasing in photoresponsive chiral liquid crystal emulsion, J. Mater. Chem. C 3 (2015) 2462–2470.
[30] R. Gupta, M. Stevenson, A. Dogariu, M.D. McGehee, J.Y. Park, V. Srdanov, A.J. Heeger, Low-threshold amplified spontaneous emission in blends of conjugated polymers, Appl. Phys. Lett. 73 (1998) 3492.
[31] M.D. McGehee, R. Gupta, S. Veenstra, E.K. Miller, M.A. Díaz-García, A.J. Heeger, Amplified spontaneous emission from photopumped films of a conjugated polymer, Phys. Rev. B 58 (1998) 7035.
[32] Q. Niu, Q. Zhang, W. Xu, Y. Jiang, R. Xia, D.D.C. Bradley, D. Li, X. Wen, Solution-processed anthracene-based molecular glasses as stable blue-light-emission laser gain media, Org. Electron. 18 (2015) 95–100.
[33] G.A. Turnbull, P. Andrew, M.J. Jory, W.L. Barnes, I.D.W. Samuel, Relationship between photonic band structure and emission characteristics of a polymer distributed feedback laser, Phys. Rev. B 64 (2001) 125122.